The Astrophysical Journal, 706:614–622, 2009 November 20 doi:10.1088/0004-637X/706/1/614

RUBIDIUM IN THE INTERSTELLAR MEDIUM

Kyle M. Walker[1,5], S. R. Federman[1,5], David C. Knauth[2,3,6], and David L. Lambert[4]
[1] Department of Physics and Astronomy, University of Toledo, Toledo, OH 43606, USA; kwalker@physics.utoledo.edu, steven.federman@utoledo.edu
[2] Franklin High School, Reisterstown, MD 21136, USA; knauth_dc2@hotmail.com
[3] Department of Physics and Astronomy, Johns Hopkins University, Baltimore, MD 21218, USA
[4] W. J. McDonald Observatory, University of Texas at Austin, Austin, TX 78712, USA; dll@astro.as.utexas.edu
Received 2009 January 2; accepted 2009 October 6; published 2009 November 3

ABSTRACT

We present observations of interstellar rubidium toward *o* Per, ζ Per, AE Aur, HD 147889, χ Oph, ζ Oph, and 20 Aql. Theory suggests that stable ^{85}Rb and long-lived ^{87}Rb are produced predominantly by high-mass stars, through a combination of the weak *s*- and *r*-processes. The ^{85}Rb/^{87}Rb ratio was determined from measurements of the Rb I line at 7800 Å and was compared to the solar system meteoritic ratio of 2.59. Within 1σ uncertainties, all directions except HD 147889 have Rb isotope ratios consistent with the solar system value. The ratio toward HD 147889 is much lower than the meteoritic value and similar to that toward ρ Oph A; both lines of sight probe the Rho Ophiuchus Molecular Cloud. The earlier result was attributed to a deficit of *r*-processed ^{85}Rb. Our larger sample suggests instead that ^{87}Rb is enhanced in these two lines of sight. When the total elemental abundance of Rb is compared to the K elemental abundance, the interstellar Rb/K ratio is significantly lower than the meteoritic ratio for all the sight lines in this study. Available interstellar samples for other *s*- and *r*- process elements are used to help interpret these results.

Key words: ISM: abundances – ISM: atoms – stars: individual (omicron Persei, zeta Persei, AE Aurigae, HD 147889, chi Ophiuchi, zeta Ophiuchi, 20 Aquilae)

1. INTRODUCTION

Rubidium isotopes ^{85}Rb and ^{87}Rb are products of the neutron capture slow (*s*-) and rapid (*r*-) processes. (^{87}Rb is unstable with the long halflife of 4.75×10^{10} years.) The *s*-process contributions come from two types of stars: the so-called main *s*-process operates in low mass asymptotic giant branch (AGB) stars with their products ejected into the interstellar medium (ISM) by the stellar wind; and the weak *s*-process occurs in the He- and C-burning shells of massive stars and distributed into the ISM primarily, it is thought, by a star's terminal supernova explosion. The *r*-process most likely occurs at the time of the supernova explosion. Of primary relevance to studies of the Rb elemental and isotopic abundances beyond the solar system is the division of responsibility for Rb synthesis between low-mass long-lived and high-mass short-lived stars or, equivalently, the relative contributions from the main *s*-process and the combination of the weak *s*-process and the *r*-process.

Dissection of the solar system abundances for Rb and adjacent elements enables fractional contributions of the weak and main *s*-processes to be estimated. Then, the *r*-process contribution is obtained as the differences between the solar system abundance and the sum of the weak and main *s*-process contributions. The most recent exercise of this kind is that reported by Heil et al. (2008) who estimated the fractional contributions of the main *s*-process to the solar system abundances of ^{85}Rb and ^{87}Rb to be 0.17 and 0.24, respectively. In other words, the relative contributions of low-mass and high-mass stars is $0.17/0.83 = 0.20$ for ^{85}Rb and $0.24/0.76 = 0.32$ for ^{87}Rb. (Heil et al. (2008) give the weak *s*-process fractional contributions as 0.24 for ^{85}Rb and 0.46 for ^{87}Rb and, then by subtraction of the two *s*-process contributions, the *r*-process contributions are 0.59 for ^{85}Rb and 0.30 for ^{87}Rb.) Earlier dissections of the solar system abundances have given somewhat different results for the relative contributions of low- and high-mass stars, e.g., Arlandini et al. (1999) gave $0.16/0.84 = 0.19$ for ^{85}Rb and $0.35/0.65 = 0.54$ for ^{87}Rb, indicating a more pronounced role of the massive stars in the synthesis of ^{87}Rb (relative to ^{85}Rb) than suggested by Heil et al. (2008). Most probably, higher weight should be given to Heil et al.'s result because it was based in part on new and accurate measurements of neutron capture cross sections, especially for the two Rb isotopes. Our study of interstellar Rb was undertaken to set observational constraints on the proposed mechanisms of Rb nucleosynthesis.

Rubidium has been analyzed in both unevolved and evolved stars. Lambert & Luck (1976) sought the Rb isotope ratio in Arcturus. Gratton & Sneden (1994) studied the abundances of neutron-rich elements in metal-poor stars, while Tomkin & Lambert (1999) considered rubidium in metal-deficient disk and halo stars. Others have examined rubidium abundances in AGB stars (Lambert et al. 1995; Abia & Wallerstein 1998; Abia et al. 2001). However, rubidium is difficult to measure in stellar atmospheres. The Rb I lines at 7800 and 7947 Å are blended with nearby lines and stellar broadening prevents the hyperfine and isotopic components from being resolved. Intrinsically, narrow interstellar lines are not hindered by these complications.

The detection of rubidium in the ISM was first reported by Jura & Smith (1981) from absorption toward the bright star ζ Oph. They used the Rb I $5s\ ^2S_{1/2}$–$5p\ ^2P_{3/2}$ line at 7800.29 Å. This is the strongest resonance line of neutral rubidium and is used for our study as well, even though most rubidium in diffuse interstellar clouds is ionized because it has a low-ionization potential of 4.177 eV. Rubidium's overall low abundance requires the use of its strongest line.

The early detection by Jura & Smith (1981) could not be confirmed by Federman et al. (1985), who also could not detect Rb I toward *o* Per nor ζ Per. Federman et al. (1985) calculated a typical 3σ upper limit in column density of $\sim 5 \times 10^9$ cm^{-2} for these lines of sight. Interstellar absorption toward these three stars is revisited in this study. More recently, Gredel et al. (2001)

[5] Guest Observer, W. J. McDonald Observatory, University of Texas at Austin, Austin, TX 78712, USA.
[6] Visiting Scientist.

Table 1
Observational Data

HD	Name	Type	V (mag)	d (pc)	Date Observed	Exposure Time (minutes)	Unreddened Star
23180	o Per	B1 III	4.98	450	2005 Dec, 2007 Jan	1470	α Leo, γ Cas
24398	ζ Per	B1 Iab	2.88	300	2005 Dec, 2007 Jan	946	α Leo, γ Cas
34078	AE Aur	O9.5 Ve	6.00	450	2005 Dec, 2007 Jan	1500	α Leo, γ Cas
147889	...	B2 III/IV	7.95	135	2006 Jun	560	α Vir
148184	χ Oph	B2 V	4.42	150	2005 May	810	α Vir, α Lyr
149757	ζ Oph	O9 V	2.58	140	2005 May, 2006 Jun	801	α Vir, α Lyr
179406	20 Aql	B3 V	5.36	375	2005 May, 2006 Jun	1055	α Vir, α Lyr

provided the first firm detections of interstellar rubidium toward Cyg OB2 Nos. 12 and 5.

The solar system isotope ratio is found from carbonaceous chondrite meteorites, with a ratio of $^{85}Rb/^{87}Rb = 2.59$ (Lodders 2003). Federman et al. (2004) found an interstellar isotope ratio toward ρ Oph A of 1.21, which differs significantly from the meteoritic value. This was the first relatively precise determination of the rubidium isotope ratio for extrasolar gas. In a recent paper, Kawanomoto et al. (2009) studied the line of sight toward HD 169454 and derived an isotope ratio that is consistent with the solar system value. The present study expands upon the results of Federman et al. (2004) and Kawanomoto et al. (2009) on the stable ^{85}Rb and long-lived ^{87}Rb isotopes.

We sought Rb absorption along seven lines of sight toward o Per, ζ Per, AE Aur, HD 147889, χ Oph, ζ Oph, and 20 Aql. These lines of sight were selected because they sample different directions in the solar neighborhood, and because other relevant data noted below are available for them. Furthermore, the cloud structure is simple with only one or two apparent components per line of sight. We explore $^{85}Rb/^{87}Rb$ ratios and compare the results to those for ρ Oph A. We also compare the elemental abundance ratio of Rb/K, as well as the $^{85}Rb/K$ and $^{87}Rb/K$ ratios, to examine whether the ^{85}Rb or ^{87}Rb abundances are lower or higher relative to the abundances seen in meteorites. Section 2 summarizes the high-resolution observations and data reduction techniques on the Rb I λ7800 line. Section 3 presents the analysis of the data and Section 4 the results, including confidence limits on the column densities. Section 5 uses the results to discuss the implications for interstellar rubidium and its nucleosynthetic production site(s). Finally, Section 6 gives the summary and conclusion.

2. OBSERVATIONS AND DATA REDUCTION

We observed the stars with the Robert G. Tull Spectrograph—formerly 2dcoudé spectrograph—(Tull et al. 1995) on the Harlan J. Smith 2.7 m telescope at McDonald Observatory from 2005 to 2007. We used the high-resolution mode with echelle grating E1 to acquire spectra on a 2048 × 2048 Tektronix CCD. Depending on the central wavelength, there were either 12 or 13 orders imaged onto the CCD and each order was around 30 Å wide. The grating was centered near 7298 Å to capture the Rb I λ7800 feature in either the eighth or ninth order. A 145 μm slit gave a resolving power of 175,000 (2.9 pixels per resolution element), as determined from the width of lines in the Th–Ar comparison spectra. The resolving power varied from 172,000 to 184,000 from night to night and from epoch to epoch. For calibration, we obtained bias and flat-field exposures at the beginning of each night. Furthermore, we acquired a set of 30-minute long dark current exposures on the first night of the observing runs. The dark images were used to determine the rate that thermal electrons accumulated on the CCD. Every 2–3 hr throughout the night we obtained a Th–Ar comparison spectrum for wavelength calibration. Also, each night we observed an unreddened star such as α Leo or γ Cas centered on the slit to see if there were any CCD blemishes not removed by the flat-fielding process. There was a seven-pixel wide CCD detector glitch in the 2005 December run that affected the spectra of ζ Per. We were unable to remove the glitch and subsequently those spectra were not used. In all other runs, the glitch did not fall on the Rb I feature. This was due to the fact that we shifted the center position of the detector slightly each night to minimize the chance of the feature falling on corrupted pixels. Individual exposures were limited to 30 minutes to minimize the presence of cosmic rays. Table 1 lists the stellar and observational parameters: HD number, name, spectral type, V magnitude, and distance in pc (obtained from the SIMBAD database, operated at CDS, Strasbourg, France), dates observed, exposure time, and unreddened stars observed.

The data were reduced using standard routines within the IRAF environment. Master bias and dark images were subtracted from all the raw object, comparison, and flat images. These images were processed further to apply the overscan strip correction. Cosmic rays were eliminated in the object and comparison images and these images, along with the master flat, were fit with a low-order polynomial that subtracted the scattered light from each order. The master flat was normalized to unity and divided into each object and comparison image and the light from each aperture was summed to form one-dimensional spectra. At this point, the spectra of the program and unreddened stars were compared to check for CCD glitches or artifacts. Typically three or more Th–Ar lines in the comparison spectra were identified per order for the wavelength solution. The rms deviation averaged 10^{-4} Å by fitting the x- and y-directions to second-order polynomials. Over the entire spectrum, there were few moderately strong lines. Two comparison spectra were assigned to each spectrum and it was corrected for dispersion. Each spectrum was then Doppler-corrected and all were summed to obtain a spectrum for each night. Each night's summed spectra were compared to make sure there were no discrepancies in the width or depth of the Rb I feature. None were present. Finally, the individual exposures for each line of sight were summed to produce seven spectra.

Table 2 gives the signal-to-noise ratio (S/N) per pixel and the equivalent width (W_λ) of the line divided by its uncertainty (σ). The equivalent width was measured using the deblending function in SPLOT of IRAF, where Voigt profiles were fit to the features. The uncertainty was calculated by dividing the full width at half-maximum (FWHM) of the Rb I feature by the average S/N in the stellar continuum. The goal was to achieve values for W_λ/σ of about 10 so that the Rb I profiles could be fitted with confidence.

Table 2
Rb I Spectra

Name	S N	W_λ/σ
o Per	3300	8.9
ζ Per	4500	10.8
AE Aur	1500	10.5
HD 147889	700	13.2
χ Oph	2100	11.6
ζ Oph	4100	16.9
20 Aql	2100	18.4

Table 3
Rb I Hyperfine Structure Component Wavelengths and f-Values

Species	λ(Å)	f-Value
^{85}Rb	7800.232	0.290
	7800.294	0.406
^{87}Rb	7800.183	0.261
	7800.321	0.435

3. ANALYSIS

The Rb I spectra were synthesized using a C++ program (J. Zsargó, modified by Knauth, hereafter called RbFits) to fit the profile, taking the instrumental width into account. RbFits took as input $V_{\rm LSR}$, the b value, and the column density, N. In order to determine the starting input velocities and b values for the RbFits program, K I parameters were used, as K I is expected to trace Rb I in diffuse interstellar gas. Whenever possible, results from the weak K I lines at 4044 and 4047 Å, whose values of W_λ are similar to those of Rb I, were adopted. Occasionally, the strong line at λ7699 was used to find the component structure, but in all cases the weak lines provided K I column densities. It is also worth noting that the K I lines have unresolved hyperfine components and are not affected by the presence of isotopes; thus their profiles are relatively simple. In fact, all the alkalis are likely to coexist in diffuse interstellar clouds (Welty & Hobbs 2001; Knauth et al. 2003; Federman et al. 2004); if the K I did not trace Rb I particularly well, ^{7}Li I and ^{6}Li I were used as a guide. The rubidium absorption toward χ Oph and 20 Aql incorporated starting values from the Li I data; all other lines of sight began their fits with K I velocities and b values. The velocities reported below are based on fits to the Rb I profile. These final Rb I velocities agree well with those determined for Li I and K I (e.g., Knauth et al. 2003). The RbFits program fit Voigt profiles to the features taking the hyperfine structure of both ^{85}Rb I and ^{87}Rb I into account. The wavelengths and f-values from Morton (2000) are given in Table 3.

When fitting the profile, RbFits calculated the lowest χ^2 by modifying the input values. Also, each input parameter of each cloud was either allowed to be held fixed or to vary. The goal was to obtain a synthesized profile where the velocity and b values for both isotopes were equal, and the column densities of each cloud formed an isotope ratio at least similar to the solar system value, 2.59. The inferred isotope ratio did not depend on the initial value of 2.0 or 2.5. At the same time, a check was performed on the reduced χ^2, which ideally should be ∼1.0. For lines of sight with one cloud, there were 43 degrees of freedom; there were 51 degrees of freedom for lines of sight with two clouds (one degree per data point of the feature minus the number of parameters being fit).

The simplest lines of sight were those that had only one cloud component, ζ Per, HD 147889, and χ Oph. The K I template for ζ Per was taken from Knauth et al. (2000), and that for χ Oph was from Knauth et al. (2003). An HD 147889 K I spectrum for the line at 7699 Å was obtained from our unpublished results and was fitted using a FORTRAN InterStellar MODelling program, ISMOD (Y. Sheffer, unpublished), because there was no cloud structure available in the literature. Using velocities, b values, and equivalent widths estimated from IRAF routines, ISMOD fit a profile to the HD 147889 data that included unresolved hyperfine structure. The results from the main component were used as the starting point for RbFits.

Federman et al. (2004) performed a synthesis with RbFits on ρ Oph A. The first step in using the RbFits program was to reproduce the results from that study. First, all six parameters were allowed to vary. From this output, both velocities were set to 1.96 km s^{-1} and both b values were set to 1.43 km s^{-1} from the solution of ^{87}Rb. RbFits was run again with these four values held fixed, only allowing the column density to vary. The resulting solution had a reduced χ^2 of 1.57, similar to the 1.43 of Federman et al. (2004). The ^{87}Rb/^{85}Rb isotope ratio for ρ Oph A was computed to be 1.22 ± 0.30, consistent with the 1.21 ± 0.30 obtained by Federman et al. (2004). Furthermore, a plot of the spectrum of ρ Oph A was created with the data and fit. A visual inspection was performed to make sure that the residuals (data minus fit) were the same inside and outside the profile.

The above technique was used to obtain syntheses for the seven new lines of sight. The basic routine was to start by varying everything and then fixing more and more parameters until the solution had a reduced χ^2 around 1.0, the residuals were consistent along the profile, and the ^{87}Rb/^{85}Rb isotope ratio was reasonable.

3.1. One-component Fits

The starting input values for χ Oph were taken from the K I and ^{7}Li I values of Knauth et al. (2003). The input velocity and b-value were 0.20 and 1.00 km s^{-1}, respectively. Because the lines are so weak, the input column density was derived from the ratio of equivalent width to column density for ρ Oph A using the simple equation

$$\frac{W_\lambda(\rho\ \text{Oph A})}{N(\rho\ \text{Oph A})} = \frac{W_\lambda(\chi\ \text{Oph})}{N(\chi\ \text{Oph})}, \quad (1)$$

where W_λ(X) is the equivalent width of the Rb I line and N is the total column density of ^{87}Rb and ^{85}Rb combined. Once the total column density was determined, it was divided so that the isotope ratio would be similar to that of the solar system. Thus, 67% of $N(\chi$ Oph) was ^{85}Rb and 33% of it was ^{87}Rb, using a ratio of 2:1 that is midway between the results for ρ Oph A (Federman et al. 2004) and the solar system (Lodders 2003). These were the column densities used for the starting point in RbFits. χ Oph has the highest reduced χ^2, but the synthesized profile fits the data well. This "ratio" technique was also used for HD 147889.

The profile for ζ Per was synthesized in three steps, following the above procedure. The starting values were taken from Knauth et al. (2000). During the second step, however, instead of using the velocity output from ^{87}Rb I, the velocity of ^{85}Rb I was more similar to that of K I and ^{7}Li I from Knauth et al. (2000). After using the velocity and b value from the solution of ^{85}Rb I, the rest of the synthesis was performed as described above. Figure 1 displays the fitted spectra toward ζ Per, χ Oph, and HD 147889.

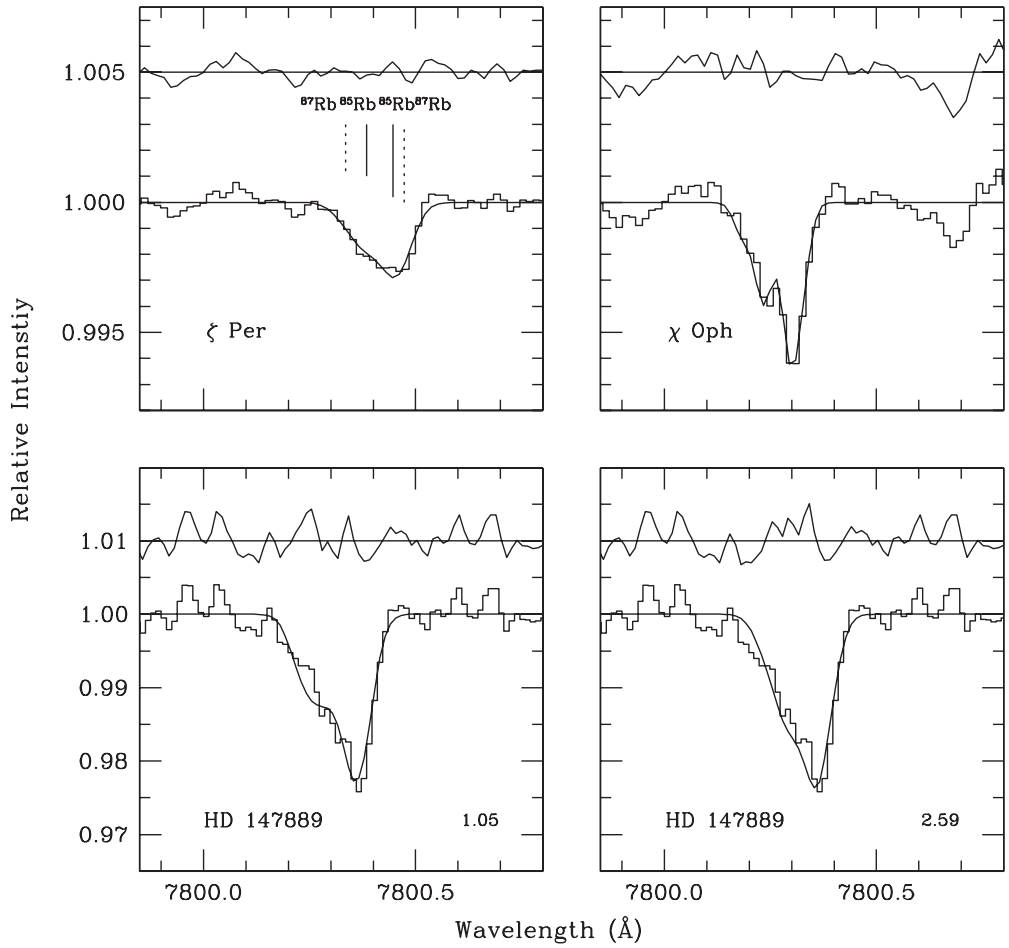

Figure 1. Synthesis of Rb I toward ζ Per, χ Oph, and HD 147889 based on one-component fits. The histogram indicates the data, while the solid line is the fit. The residuals (data minus fit) are offset to 1.005, except for HD 147889, where they are offset to 1.01. The vertical solid lines above the spectrum of ζ Per indicate ^{85}Rb while the dashed lines indicate ^{87}Rb. The lengths show the relative line strengths. The feature in χ Oph at 7800.68 Å is a glitch that did not compromise our spectrum. Note the expanded scale for HD 147889. The bottom left panel is fitted with a ^{85}Rb/^{87}Rb ratio of 1.05, while the bottom right panel is fit with the solar system ratio; the isotope ratio is given in the lower right corner.

3.2. Two-component Fits

The profiles of the four lines of sight with two components were more difficult to synthesize. The starting values did not affect the outcome of the one-component fits, whereas the simple "ratio" technique of dividing equivalent widths by column densities was no longer valid because the profiles were more complex, each having eight components (two hyperfine components for each isotope for each cloud). The program needed better starting values from other data (velocity separations, etc.), especially for the column densities. There are two ways to solve this problem.

For the first way, a list of abundances of Rb I and K I was created from lines of sight with one component: χ Oph, ζ Per, HD 147889, ρ Oph A, and the two lines of sight from Gredel et al. (2001), and Cyg OB No. 5 and No. 12. The K I column densities were obtained from Knauth et al. (2000; ζ Per), Knauth et al. (2003; χ Oph), Federman et al. (2004; ρ Oph A, Cyg OB Nos. 5 and 12), and derived from unpublished observations (HD 147889). An average of the N(Rb I)/N(K I) ratios for each line of sight yielded 9.5×10^{-4}. At this preliminary stage of the analysis for AE Aur, the component structure and N(K I) come from the synthesis of λ7699 from unpublished data. For all other directions, N(K I) is obtained from the weak line at λ4044. Using the above average and knowing K I for the four lines of sight in the current study, one could work backwards to find N(Rb I). Then using N(Rb I) as the total column density for a given line of sight and the cloud fractions from Knauth et al. (2003) for o Per, ζ Oph, and 20 Aql as well as our results for AE Aur, the column densities for each cloud were obtained.

For example, o Per has a total K I column density of 1.04×10^{12} cm^{-2}. Then, according to Federman et al. (2004) and assuming equal depletion of Rb and K although the elements have somewhat different condensation temperatures (Lodders 2003),

$$\left[\frac{A_g(\mathrm{Rb})}{A_g(\mathrm{K})}\right] = \left[\frac{N(\mathrm{Rb\ I})}{N(\mathrm{K\ I})}\right]\left[\frac{G(\mathrm{Rb\ I})}{G(\mathrm{K\ I})}\right]\left[\frac{\alpha(\mathrm{K\ I})}{\alpha(\mathrm{Rb\ I})}\right], \quad (2)$$

where A_g(Rb)/A_g(K) is the elemental abundance ratio, G(X) is the photoionization rate corrected for grain attenuation, and α(X) is the rate coefficient for radiative recombination. We adopted the same sources for the atomic data used by Federman et al. (2004) to infer photoionization rates for Rb I of 3.42×10^{-12} s^{-1} and for K I of 8.67×10^{-12} s^{-1}. For Rb I, the theoretical calculations of Weisheit (1972) give cross sections for 1150–1250 Å, which were scaled to the measurements of Marr & Creek (1968) at longer wavelengths. The cross sections for K I are taken from the measurements of Hudson & Carter (1965), Hudson & Carter (1967), Marr & Creek (1968), and Sandner et al. (1981). For wavelengths below 1150 Å, there

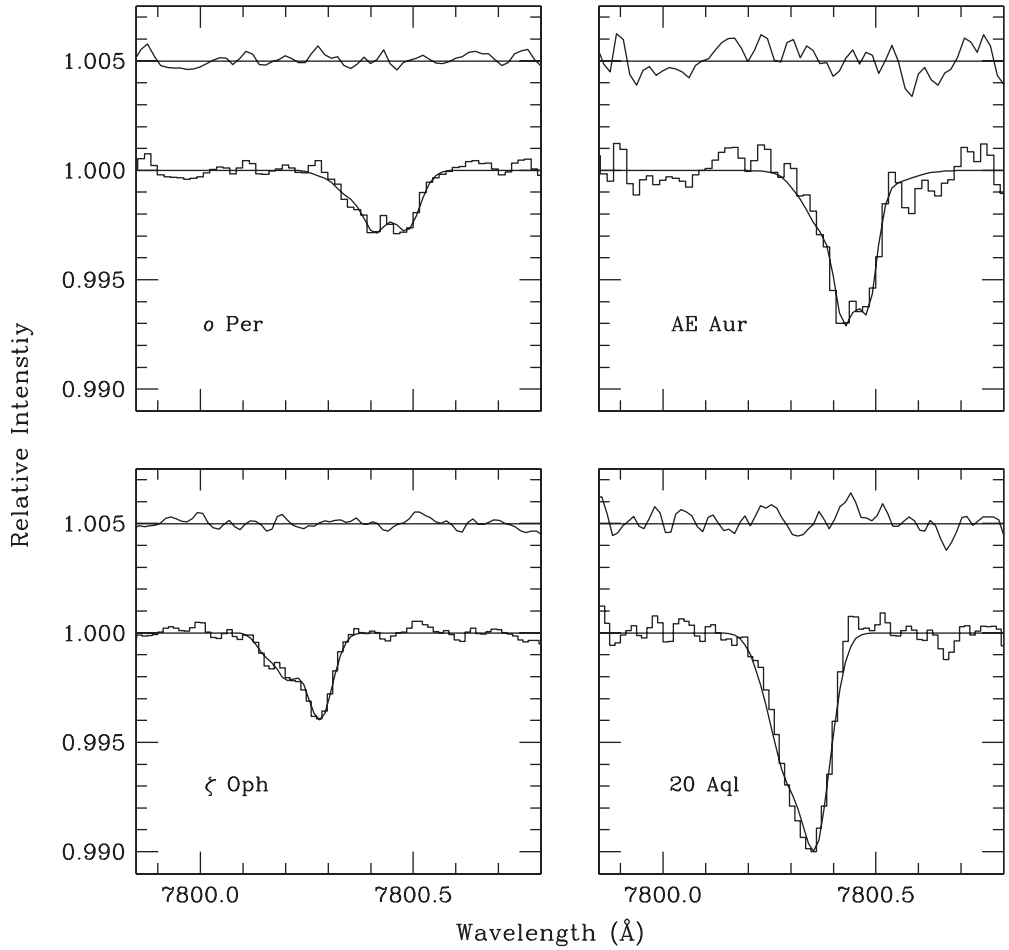

Figure 2. Synthesis of Rb I toward *o* Per, AE Aur, ζ Oph, and 20 Aql based on two-component fits. Same as Figure 1.

is no differential attenuation because the ionization potentials are similar (4.18 eV for Rb I and 4.34 eV for K I). Based on these cross sections, a 13% correction was applied to G(Rb I) for $\lambda < 1150$ Å. The rate coefficients for radiative electron recombination are similar, within 10% of one another (Wane 1985; Péquignot & Aldrovandi 1986; Wane & Aymar 1987), and so the ratio of the rate coefficients is ∼1. The ratio of the photoionization rates is 0.394.

For *o* Per, we can solve for N(Rb I), which is 2.51×10^9 cm^{-2}. Then, we multiplied this column density by the percentage in each cloud (taken from Knauth et al. 2003), 14% and 86% for the clouds at 3.96 and 6.98 km s^{-1}, respectively. Assuming the ratio in each component would be similar to the solar system value, the relative amounts of the isotopes were separated. The result was that four starting column densities were created.

The second way to obtain starting column densities was to perform a one component fit on the data, as in the case of ζ Oph. This one component fit provided a coarse estimate of a weighted velocity, b value, and column density for each isotope. The isotopes were then split into their resultant components according to Knauth et al. (2003). The resulting spectra with two components are shown in Figure 2.

4. RESULTS

4.1. The Rubidium Isotope Ratio

The Rb isotope ratio is expected to be independent of the two principal effects that hamper the extraction of the Rb/H ratio from the Rb I equivalent widths, namely, the large degree of ionization of Rb to Rb$^+$, and the loss of Rb onto grains. Table 4 shows the final solutions for the lines of sight in our survey. It lists the resulting velocities, column densities, b-values, ^{85}Rb/^{87}Rb ratios, and reduced χ^2s, calculated from the RbFits program. The b-values range from 0.45 to 1.46 km s^{-1}; while the larger values may indicate the presence of unresolved structure, similar values have been reported previously (e.g., Knauth et al. 2003). The reduced χ^2s are all around 1.0. The uncertainties for each cloud were calculated using the FWHM, derived from the b value, and S/N of each spectrum. For such weak lines, the same fractional uncertainty applies to the column densities also. These were propagated in the usual way to place uncertainties on the inferred isotope ratios. When 2σ was greater than the equivalent widths for the ^{87}Rb line, only lower limits to the ratio are possible. All lines of sight are consistent with the solar system value, 2.59, as determined from meteorites, except for HD 147889 and the previously measured ρ Oph A (Federman et al. 2004).

We investigated the sensitivity of our results for HD 147889 by attempting to fit the Rb I profile with the solar system ratio. Various combinations of keeping $V_{\rm LSR}$ and b-value fixed were attempted. All gave similar results, with reduced χ^2s from 1.62 to 1.81 compared to our preferred synthesis with 1.44. We performed analyses of the Rb isotope ratio toward HD 147889 of a single component fit in two additional ways. In the first analysis, all profile synthesis parameters were allowed to vary. For the second analysis only the ^{85}Rb and ^{87}Rb column densities

Table 4
Isotope Ratios

Star	Isotope	V_{LSR} (km s^{-1})	N (cm^{-2})	b-Value (km s^{-1})	^{85}Rb/^{87}Rb Ratio	Reduced χ^2
o Per	87	4.05	$<1.00 \times 10^8$	0.84		
	85	4.05	$(2.72 \pm 0.35) \times 10^8$	0.84	>2.72	
	87	7.07	$(2.70 \pm 0.30) \times 10^8$	1.06		
	85	7.07	$(6.40 \pm 0.71) \times 10^8$	1.06	2.37 ± 0.79	0.72
ζ Per	87	5.88	$(3.29 \pm 0.29) \times 10^8$	1.46		
	85	5.88	$(7.49 \pm 0.67) \times 10^8$	1.46	2.28 ± 0.59	1.75
AE Aur	87	5.34	$<3.00 \times 10^8$	1.03		
	85	5.34	$(8.23 \pm 1.07) \times 10^8$	1.03	>2.74	
	87	7.30	$(4.50 \pm 0.59) \times 10^8$	1.00		
	85	7.30	$(1.13 \pm 0.15) \times 10^9$	1.00	2.52 ± 1.03	1.06
HD 147889	87	2.04	$(4.21 \pm 0.35) \times 10^9$	1.33		
	85	2.04	$(4.33 \pm 0.36) \times 10^9$	1.33	1.03 ± 0.21	1.44
χ Oph	87	0.13	$(4.85 \pm 0.38) \times 10^8$	0.46		
	85	0.13	$(1.27 \pm 0.11) \times 10^9$	0.46	2.62 ± 0.63	2.06
ζ Oph	87	−1.21	$(2.99 \pm 0.25) \times 10^8$	0.45		
	85	−1.21	$(4.72 \pm 0.39) \times 10^8$	0.45	1.58 ± 0.32	
	87	−0.17	$(1.54 \pm 0.21) \times 10^8$	0.59		
	85	−0.17	$(3.19 \pm 0.43) \times 10^8$	0.59	2.07 ± 0.78	0.94
20 Aql	87	2.06	$(7.26 \pm 0.53) \times 10^8$	1.28		
	85	2.06	$(2.05 \pm 0.15) \times 10^9$	1.28	2.82 ± 0.68	
	87	3.04	$<2.42 \times 10^8$	1.19		
	85	3.04	$(6.06 \pm 0.31) \times 10^8$	1.19	>2.51	0.90

were allowed to vary. For the second synthesis, the velocity and the Doppler broadening parameters were fixed to those determined from the profile fit to the measured interstellar K I line. This led to an improved reduced χ^2 over that of the freely varying profile synthesis. Application of an F-test (Lupton 1993, p. 100) shows the improvement in χ^2 is justified to the 68% confidence level. In order to test whether our single component fit of the Rb isotope ratio is potentially two components, a subsequent analysis was performed. This analysis led to an overall improvement in the reduced χ^2. An F-test shows that a second component is justified at the 80% confidence level. The synthesis based on changing V_{LSR} appears in the lower right panel of Figure 1. The fit on the blue side is poorer and below the data points, which is evidenced by the residuals within the left side of the profile not appearing random.

4.2. Comparison with Elemental Potassium Abundance

Neutral Rb is expected to follow the spatial trend of neutral K in interstellar clouds because they have similar ionization potentials and chemical properties, and so a determination of the interstellar elemental Rb/K ratio from Equation (2) compared to the meteoritic value may provide new insights into the production of neutron capture elements. High-resolution surveys have been performed for interstellar Li I (Knauth et al. 2003), Na I (Welty et al. 1994), and K I (Welty & Hobbs 2001) absorption. Knauth et al. (2003) conclude that the elemental Li/K abundance ratio is consistent with the solar system value, and Welty & Hobbs (2001) also confirm the essentially linear relationship between the total column densities of Li I, Na I, and K I. It seems that Li, Na, and K are likely depleted by comparable amounts in the relatively cool, dense regions where the neutral species are concentrated (Welty & Hobbs 2001). Thus, we apply Equation (2) with confidence.

Using this equation Rb/K, as well as ^{85}Rb/K and ^{87}Rb/K, were determined and the results are presented in Table 5. The results for ρ Oph A (Federman et al. 2004) and the solar system values (Lodders 2003) are shown for comparison. The K I column densities were obtained from the weak line at 4044 Å, except for AE Aur, where we adopted the unpublished λ4047 results of P. Boissé. The K I value for HD 147889 comes from Welty & Hobbs (2001).

Table 5
Abundance Ratios from the Neutral Species

Star	V_{LSR} (km s^{-1})	^{85}Rb/^{87}Rb	Rb/K[a]	^{85}Rb/K[a]	^{87}Rb/K[a]
o Per	4.05	>2.72	10.0 ± 1.0	7.3 ± 1.3	<2.7
	7.07	2.37 ± 0.79	4.0 ± 1.1	2.8 ± 0.7	1.2 ± 0.4
ζ Per	5.88	2.28 ± 0.59	6.1 ± 0.6	4.2 ± 0.3	1.9 ± 0.3
AE Aur	5.34	>2.74	3.0 ± 0.6[b]	2.2 ± 0.8[b]	<0.8[b]
	7.30	2.52 ± 1.03	6.1 ± 1.3[b]	4.3 ± 0.9[b]	1.7 ± 0.4[b]
HD 147889	2.04	1.03 ± 0.21	8.6 ± 1.3[c]	4.4 ± 0.7[c]	4.3 ± 0.6[c]
χ Oph	0.13	2.62 ± 0.63	5.4 ± 0.7	3.9 ± 0.4	1.5 ± 0.3
ζ Oph	−1.21	1.58 ± 0.32	5.7 ± 0.6	3.5 ± 0.3	2.2 ± 0.3
	−0.17	2.07 ± 0.78	6.4 ± 1.1	4.3 ± 0.7	2.1 ± 0.5
20 Aql	2.06	2.82 ± 0.68	7.0 ± 0.7	5.2 ± 0.5	1.8 ± 0.3
	3.04	>2.51	5.2 ± 0.7	3.7 ± 0.8	<1.5
ρ Oph A	...	1.21 ± 0.30[d]	13.0 ± 3.0[d]	7.3 ± 1.2[d]	6.1 ± 1.3[d]
Solar System	...	2.59[e]	17.8 ± 3.7[e]	12.9[e]	4.9[e]

Notes.
[a] The values for Rb/K, ^{85}Rb/K, and ^{87}Rb/K are in units of 10^{-4}.
[b] From data provided by P. Boissé, unpublished.
[c] K I values are from Welty & Hobbs (2001).
[d] Federman et al. (2004).
[e] Lodders (2003).

The seven new lines of sight given in Table 5 all show a deficit in the ratios relative to potassium, with the possible exception of ^{87}Rb/K toward ρ Oph A. Relative to the meteoritic ratios, we find Rb/K = 34%, ^{85}Rb/K = 32%, and ^{87}Rb/K = 36%. These ratios are inferred from Equation (2), which does not

allow for different depletions onto grains. As mentioned below, the condensation temperature for Rb is lower than that for K; if only depletion mattered, one would expect a higher Rb/K ratio, contrary to the observational results. Note that ^{85}Rb/K toward o Per seems to be larger than the other ratios, and that the anomalously large ratios of ^{87}Rb/K (HD 147889 and ρ Oph A) are not included in the above averages.

5. DISCUSSION

5.1. Comparison with Previous Results

The first limits on interstellar N(Rb I) come from Federman et al. (1985), who searched for absorption toward the stars o Per, ζ Per, and ζ Oph, but did not detect any to a 3σ limit of $\leqslant$1.5 mÅ. The resulting limits on N(Rb I) and Rb/K are found to be typically $\leqslant 5 \times 10^{9}$ cm^{-2} and $\leqslant 1.5 \times 10^{-3}$ (Federman et al. 2004). In all cases, our detections yield values 30%–50% of the upper limits.

Gredel et al. (2001) found column densities toward Cyg OB2 Nos. 5 and 12 of $N(\mathrm{Rb\,I}) = (7 \pm 2) \times 10^{9}$ cm^{-2} and $N(\mathrm{Rb\,I}) = (13 \pm 2) \times 10^{9}$ cm^{-2}, respectively. Combining these results with the high-resolution K I λ7699 spectra of McCall et al. (2002), Federman et al. (2004) derived values for N(K I) of the three main molecular components to be 9.4(7.7) $\times$ 10^{11}, 8.1(12) $\times$ 10^{11}, and 6.9(16) $\times$ 10^{11} cm^{-2} for the gas toward Cyg OB2 No. 5(12). Thus, Rb/K is 14×10^{-4} for No. 5 and 12×10^{-4} for No. 12. Rb/K for ρ Oph A is $(13 \pm 3) \times 10^{-4}$ (Federman et al. 2004). These three lines of sight appear to have Rb/K values about a factor of 2 higher than the average of our 11 clouds, $(6.1 \pm 1.2) \times 10^{-4}$. However, significant uncertainty remains in extracting elemental abundances toward the stars in Cyg OB2 because a blended, optically thick line was used to obtain the K I column density. Our analyses, and those of Snow et al. (2008), for HD 147889 indicate that the weaker line at 4044 Å yields a higher K I column density, leading to a smaller Rb/K ratio. Furthermore, the difference for the gas toward ρ Oph A is within $\sim 2\sigma$ of the results for our other lines of sight. Thus, all interstellar results appear smaller than the solar system value of $(18 \pm 4) \times 10^{-4}$.

From the Rb I detection toward ρ Oph A, Federman et al. (2004) suggested that there was a deficit of r-processed material because ^{87}Rb/K seemed to have the meteoritic value, while ^{85}Rb/K was considerably less than the solar system value. This is also true toward HD 147889. These two lines of sight are near one another; the anomalously low ^{85}Rb/^{87}Rb ratios seem to arise from sampling the Rho Ophiuchus Molecular Cloud. For the other lines of sight, our sample indicates that both ^{85}Rb and ^{87}Rb have a deficit relative to K in the ISM of $\sim$66%. However, the gas in the Rho Ophiuchus Molecular Cloud appears to be enriched in ^{87}Rb.

Kawanomoto et al. (2009) recently published results for the direction toward HD 169454. Their isotope ratio (^{85}Rb/^{87}Rb > 2.4) is consistent with the meteoritic value, which again highlights the unusual values that we found for the Rho Ophiuchus Molecular Cloud. Their Rb/K ratio also reveals a deficit compared to the meteoritic ratio. It is worth noting that Kawanomoto et al. make comparisons with a solar system ratio at its formation by accounting for the decay of ^{87}Rb over 4.55 Gyr. Their estimate of the original ratio is 2.43.

5.2. Interstellar Results on Neutron-capture Elements

The elemental abundances of Ge, Kr, Cd, and Sn seen in our sample of diffuse clouds, for which sufficient data exist, may provide an answer, because they are also synthesized through neutron capture. For each of these elements, the dominant ion is observed. In the solar system about 10% of Ge, 20% of Kr, 50% of Cd, and 70% of Sn are produced via the main s-process (Beer et al. 1992; Raiteri et al. 1993; Arlandini et al. 1999; Heil et al. 2008); massive stars through a combination of weak s-process and r-process are responsible for the remaining fractions. When corrected for the f-value adopted by Cartledge et al. (2006), Cardelli et al. (1991) obtain N(Ge)/N(H) of $(4.9 \pm 0.5) \times 10^{-10}$ for ζ Oph, while Lodders (2003) gives $(4.2 \pm 0.5) \times 10^{-9}$ for the solar system. Cartledge et al. (2003) find N(Kr)/N(H) to be $(9.33 \pm 1.14) \times 10^{-10}$ for ζ Per and $(7.94 \pm 0.97) \times 10^{-10}$ for ζ Oph, whereas the theoretical solar system abundance from Lodders (2003) is $(19.05 \pm 3.81) \times 10^{-10}$. Sn was measured by Sofia et al. (1999), who found N(Sn)/N(H) of $(7.41 \pm 3.18) \times 10^{-11}$ for ζ Per, $(8.13 \pm 0.98) \times 10^{-11}$ for χ Oph, $(9.12 \pm 2.65) \times 10^{-11}$ for ζ Oph, and $(5.75 \pm 0.95) \times 10^{-11}$ for ρ Oph A. The solar system abundance is $(12.88 \pm 1.24) \times 10^{-11}$ (Lodders 2003). Finally, there is one line of sight among our sample that has measured Cd, ζ Oph, where N(Cd)/N(H) is $(5.50 \pm 1.60) \times 10^{-11}$ (Sofia et al. 1999). The solar system value for this element is $(5.50 \pm 0.38) \times 10^{-11}$ (Lodders 2003). Taking into account the uncertainties, all these values are likely to be lower than the solar system values.

For these relatively dense lines of sight, depletion onto grains, not nucleosynthetic processes, could be the cause for the deficits. It is better to consider the gas phase abundances for low density, warm gas. The condensation temperatures for Ge, Kr, Cd, Sn, and Rb are 734, 52, 652, 704, and 800 K, respectively (Lodders 2003). The survey by Cartledge et al. (2006) indicates an interstellar Ge abundance that is 25% the meteoritic value. With such a low condensation temperature, Kr should not be depleted toward any line of sight. However, the average abundance of Kr found by Cartledge et al. (2003) is $\sim$50% of the solar system value. The results on Cd and Sn (Sofia et al. 1999) reveal a different trend. For low-density lines of sight, neither element shows any depletion onto grains. There is even a hint that the Sn abundance for these directions is greater than the solar system value. The deficit of Rb relative to K cannot be explained by depletion onto grains resulting from a higher condensation temperature, because Li, Na, and K have even higher values (1135, 953, and 1001 K) according to Lodders (2003), and the Li/K and Na/K elemental ratios are similar to meteoritic values (Welty & Hobbs 2001; Knauth et al. 2003).

The depletion patterns of Ge, Kr, and Rb on the one hand, and Cd and Sn on the other, cannot be attributed to imprecise oscillator strengths. According to Morton (2003), the f-values used to study interstellar Kr I, Rb I, and Cd II are well known from laboratory measurements. The same applies to Sn II as a result of the experimental results of Schectman et al. (2000). Morton (2003) recommends the theoretical value of Biémont et al. (1998) for the Ge II line at 1237 Å. While no more recent theoretical or experimental determinations are available at the present time, the dichotomy noted above would still be present if the results on interstellar Ge were not included.

A summary of the depletion patterns for the five elements appears in the top panel of Figure 3. Observational results for the amount of depletion onto grains both for low and high density clouds is shown. Each survey used to construct this figure (Cartledge et al. 2003 for Kr; Cartledge et al. 2006 for Ge; our results for Rb; Sofia et al. 1999 for Cd and Sn) indicate typical observational scatter of about 0.1 dex in the quoted depletion. Although T_{cond} is similar for Ge, Rb, Cd, and Sn, the

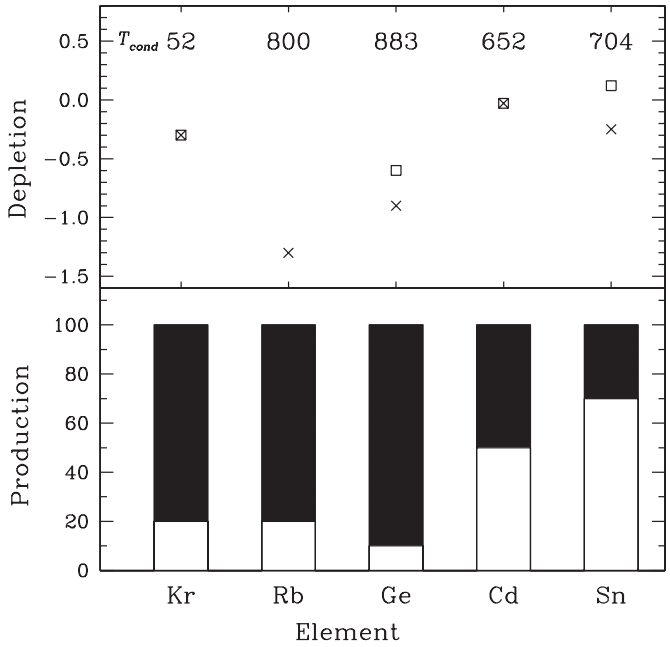

Figure 3. Upper panel depicts depletion for warm gas (squares) and cold gas (×) for Ge, Kr, Rb, Cd, and Sn along with their condensation temperatures. The uncertainties for the measured abundances are smaller than the symbols. The two groupings in production mainly from massive stars and mainly from low-mass stars are ordered by condensation temperature. The bottom panel shows production from massive stars (shaded bars) and low mass stars (white bars).

depletion patterns for Cd and Sn are strikingly different than those for Ge and Rb, even when the intrinsic scatter in plots of depletion versus $T_{\rm cond}$ are considered. Furthermore, there is less depletion for Cd and Sn than for Kr, a noble gas.

A closer look at the production routes for these *n*-capture nuclides offers a promising solution. This is highlighted in the bottom panel of Figure 3, where the white bar indicates production by low-mass stars and the shaded bar indicates massive stars. The solar system abundances for the elements Cd and Sn are believed to arise predominantly by the main *s*-process involving low-mass AGB stars (Beer et al. 1992; Raiteri et al. 1993; Arlandini et al. 1999), and they have reduced levels of depletion in the ISM. On the other hand, elements synthesized by the weak *s*-process and the *r*-process that occur in massive stars (Beer et al. 1992; Raiteri et al. 1993; Arlandini et al. 1999; The et al. 2007; Heil et al. 2008) appear to show interstellar abundances significantly lower than seen in the solar system. This possible reduction in the contribution of massive stars to interstellar abundances for *n*-capture elements contrasts with recent results for lighter elements. For instance, Przybilla et al. (2008) provide abundances for several elements in unevolved, early-type B stars that are indistinguishable from those found for the Orion Nebula (Esteban et al. 2004) and the sun (Asplund et al. 2005). The enhancement of ^{87}Rb in the Rho Ophiuchus Molecular Cloud remains puzzling. Our inferences may not be appropriate if Galactic chemical evolution altered the mix of *s*- and *r*-processed material from 4.5 Gyr ago when the solar system formed to the ISM of today. While we are not aware of predictions of the evolution of Rb and its isotopes, the weak *s*-process and *r*-process from Type II SN might be tied to the evolution of O or Mg or Si, while the main *s*-process to products of AGB stars such as Y or Ba.

Further efforts in a number of areas will likely improve our understanding. Data on interstellar Ga, As, and Pb—other *n*-capture nuclides—are available, but as of now it is more difficult to disentangle the effects of nucleosynthesis from depletion onto grains for them. Once this is accomplished, the unexpected results on Rb and its isotopes will likely be clarified. A more complete set of theoretical results, covering all isotopes of interest and based on modern stellar codes (e.g., The et al. 2007; Heil et al. 2008), are needed as well. We also see a need for theoretical studies into the evolution of these elements and their isotopes.

6. SUMMARY AND CONCLUSIONS

The interstellar ^{85}Rb/^{87}Rb ratio was measured along seven lines of sight, *o* Per, ζ Per, AE Aur, HD 147889, χ Oph, ζ Oph, and 20 Aql. Using K I absorption as a guide, the spectra were synthesized to find the velocity, column density, and *b*-value of each cloud. Most clouds had ratios that agreed, within mutual uncertainties, with the solar system value of 2.59. The gas toward HD 147889 had a lower ^{85}Rb/^{87}Rb ratio (1.03 ± 0.21) and a higher elemental ratio (8.6 ± 1.3), suggesting that ^{87}Rb is enhanced in this direction, consistent with the previous results for ρ Oph A (Federman et al. 2004). The anomalous ratios appear to arise within the Rho Ophiuchus Molecular Cloud. Furthermore, a comparison of interstellar Rb to K shows that the gas in the solar neighborhood appears to be significantly underabundant in rubidium, even after considering uncertainties in ionization balance and level of depletion. An examination of other species, such as Ge, Kr, Cd, and Sn, seems to suggest nuclides synthesized by the *n*-capture processes occurring in massive stars (weak *s* and *r*) have lower interstellar abundances than expected. Larger samples for several *n*-capture elements, from both observation and theory, will help clarify the cause for this.

We thank Dr. Y. Sheffer for his help with his program ISMOD. We acknowledge the use of the DIB database of Professor D. York at the University of Chicago, from which promising directions were noted. We also thank Prof. P. Boissé for the AE Aur K I λ4047 spectrum. D.L.L. thanks the Robert A. Welch Foundation of Houston for their support through grant number F-634. We made use of the SIMBAD database, operated at Centre de Donées Astronomiques de Strasbourg, Strasbourg, France.

REFERENCES

Abia, C., Busso, M., Gallino, R., Dominguez, I., Straniero, O., & Isern, J. 2001, ApJ, 559, 1117
Abia, C., & Wallerstein, G. 1998, MNRAS, 293, 89
Arlandini, C., Käppeler, F., Wisshak, K., Gallino, R., Lugaro, M., Busso, M., & Straniero, O. 1999, ApJ, 525, 886
Asplund, M., Grevesse, N., & Sauval, A. J. 2005, in ASP Conf. Ser., 336, Cosmic Abundances as Records of Stellar Evolution and Nucleosynthesis in honor of David L. Lambert, ed. T. G. Barnes, III & F. N. Bash (San Francisco, CA: ASP), 25
Beer, H., Walker, G., & Käppeler, F. 1992, ApJ, 389, 784
Biémont, E., Morton, D. C., & Quinet, P. 1998, MNRAS, 297, 713
Cardelli, J. A., Savage, B. D., & Ebbets, D. C. 1991, ApJ, 383, 23
Cartledge, S. I. B., Lauroesch, J. T., Meyer, D. M., & Sofia, U. J. 2006, ApJ, 641, 327
Cartledge, S. I. B., Meyer, D. M., & Lauroesch, J. T. 2003, ApJ, 597, 408
Esteban, C., Peimbert, J., García-Rojas, J., Ruiz, M. T., Peimbert, A., & Rodríguez, M. 2004, MNRAS, 355, 229
Federman, S. R., Knauth, D. C., & Lambert, D. L. 2004, ApJ, 603, 105
Federman, S. R., Sneden, C., Schempp, W. V., & Smith, W. H. 1985, ApJ, 290, 55
Gratton, R. G., & Sneden, C. 1994, A&A, 287, 927
Gredel, R., Black, J. H., & Yan, M. 2001, A&A, 375, 553

Heil, M., Käppeler, F., Uberseder, E., Gallino, R., Bisterzo, S., & Pignatari, M. 2008, Phys. Rev. C, 78, 025802
Hudson, R. D., & Carter, V. L. 1965, Phys. Rev. A, 139, 1426
Hudson, R. D., & Carter, V. L. 1967, J. Opt. Soc. Am., 57, 1471
Jura, M., & Smith, W. H. 1981, ApJ, 251, 43
Kawanomoto, S., Aoki, W., Kajino, T., & Mathews, G. T. 2009, ApJ, 698, 509
Knauth, D. C., Federman, S. R., & Lambert, D. L. 2003, ApJ, 586, 268
Knauth, D. C., Federman, S. R., Lambert, D. L., & Crane, P. 2000, Nature, 405, 656
Lambert, D. L., & Luck, R. E. 1976, The Observatory, 96, 100
Lambert, D. L., Smith, V. V., Fusso, M., Gallino, R., & Straniero, O. 1995, ApJ, 450, 302
Lodders, K. 2003, ApJ, 591, 1220
Lupton, R. 1993, Statistics in Theory and Practice (Princeton, NJ: Princeton Univ. Press)
Marr, G. V., & Creek, D. M. 1968, Proc. R. Soc. A, 304, 233
McCall, B. J., et al. 2002, ApJ, 567, 391
Morton, D. C. 2000, ApJS, 130, 403
Morton, D. C. 2003, ApJS, 149, 205
Péquignot, D., & Aldrovandi, S. M. V. 1986, A&A, 161, 169
Przybilla, N., Nieva, M.-F., & Butler, K. 2008, ApJ, 688, 103
Raiteri, C. M., Gallino, R., Busso, M., Neuberger, D., & Kappeler, F. 1993, ApJ, 419, 207
Sandner, W., Gallagher, T. F., Safinya, K. A., & Gounand, F. 1981, Phys. Rev. A, 23, 2732
Schectman, R. M., Cheng, S., Curtis, L. J., Federman, S. R., Fritts, M. C., & Irving, R. E. 2000, ApJ, 542, 400
Snow, T. P., Destree, J. D., & Welty, D. E. 2008, ApJ, 679, 512
Sofia, U. J., Meyer, D. M., & Cardelli, J. A. 1999, ApJ, 522, 137
The, L.-S., El Eid, M. F., & Meyer, B. S. 2007, ApJ, 655, 1058
Tomkin, J., & Lambert, D. L. 1999, ApJ, 523, 234
Tull, R. G., MacQueen, P. J., Sneden, C., & Lambert, D. L. 1995, PASP, 107, 251
Wane, S. 1985, J. Phys. B, 18, 3881
Wane, S., & Aymar, M. 1987, J. Phys. B: At. Mol. Opt. Phys., 20, 2657
Weisheit, J. C. 1972, Phys. Rev. A, 5, 1621
Welty, D. E., & Hobbs, L. M. 2001, ApJS, 133, 345
Welty, D. E., Hobbs, L. M., & Kulkarni, V. P. 1994, ApJ, 436, 152